

LETTER TO THE EDITOR

A benchmark companion at the hydrogen-burning limit imaged in the core cluster of the Fornax-Horologium association

Pengyu Liu^{1,2,3}, Beth A. Biller^{2,3}, Matthew A. Kenworthy¹, Clémence Fontanive⁴, Ronan M. P. Kerr⁵, Tomas Stolker¹, and Christian Ginski⁶

¹ Leiden Observatory, Leiden University, PO Box 9513, 2300 RA Leiden, The Netherlands
e-mail: pengyu.liu@ed.ac.uk

² SUPA, Institute for Astronomy, University of Edinburgh, Royal Observatory, Blackford Hill, Edinburgh EH9 3HJ, UK

³ Centre for Exoplanet Science, University of Edinburgh, Edinburgh, UK

⁴ Trotter Institute for Research on Exoplanets, Université de Montréal, Montréal, H3C 3J7, Québec, Canada

⁵ Dunlap Institute for Astronomy & Astrophysics, University of Toronto, Toronto, ON M5S 3H4, Canada

⁶ School of Natural Sciences, Centre for Astronomy, University of Galway, Galway H91 CF50, Ireland

Received 14 February 2025 / Accepted 21 March 2025

ABSTRACT

Context. Low-mass stellar and substellar companions are indispensable objects for verifying evolutionary models that transition from low-mass stars to planets. Their formation is likely also affected by the surrounding stellar environment. The Fornax-Horologium (FH) association is a recently classified young association in the solar neighbourhood with a dissolving open cluster in its centre. It has not been searched widely for substellar companions and exoplanets with direct imaging.

Aims. We search for companions of stars in the FH and investigate the formation and evolution of companions during the expansion and dissolution of a star cluster.

Methods. We conduct a direct-imaging survey of 49 stars in FH with VLT/SPHERE.

Results. We present HD 24121B, a companion at the hydrogen-burning limit that orbits star HD 24121 in the core cluster of the FH. The companion is located at a projected angular separation of 2.082 ± 0.004 arcsec from the central star and has contrasts of $\Delta H2 = 5.07 \pm 0.05$ mag and $\Delta H3 = 4.98 \pm 0.05$ mag. We estimate a photometric mass of $74.9 \pm 7.5 M_J$ for HD 24121B, which places it at the boundary of brown dwarfs and low-mass stars. It is a new benchmark object for evolutionary models at the hydrogen-burning boundary, especially at the age of 30–40 Myr. Orbital fitting with joint Gaia and SPHERE relative astrometry found a high eccentricity for HD 24121B. This suggests that it may have undergone dynamic scattering. Future chemical composition measurements such as high-resolution spectroscopic observations will provide more clues on its formation history.

Key words. techniques: high angular resolution - planets and satellites: detection - brown dwarfs - stars: low-mass - stars: individual:: HD 24121 - open clusters and associations: individual:: Fornax-Horologium association

1. Introduction

The masses of brown dwarfs are intermediate between those of low-mass stars and planets. Brown dwarfs can serve as testbeds for substellar evolutionary models and formation mechanisms. Direct-imaging surveys have discovered dozens of brown dwarf companions, such as PZ Tel B (Biller et al. 2010), CD 35-2722B (Wahhaj et al. 2011), HD 1160B (Nielsen et al. 2012), HR 2562B (Konopacky et al. 2016), and HD 4747B (Crepp et al. 2016). Unlike low-mass planets, the formation of these heavy brown dwarfs via core accretion (Pollack et al. 1996) in the protostellar and protoplanetary discs is challenging. They are more likely formed via direct collapse in the disc, such as by disc fragmentation (Boss 1997). Moreover, 40-50% of the directly imaged substellar companions are more than 100 au from away from their host stars¹. The stellar environment may affect the formation of wide-orbit companions via gravitational instability and dynamical interactions (e.g., Forgan et al. 2015; Zheng et al. 2015; Fujii & Hori 2019). There are tentative findings on the frequency of stellar and brown dwarf companions that vary in different re-

gions, but they remain limited to small samples (Gratton et al. 2024, 2025).

Past and current direct-imaging surveys mainly focus on nearby young moving groups and OB associations (e.g., Biller et al. 2013; Nielsen et al. 2019; Desidera et al. 2021). In recent years, several new young clusters and associations have been established. The χ^1 Fornacis cluster (XFOR) was first compiled in a catalogue of open clusters with the name of Alessi 13 by Dias et al. (2002). In this cluster, 108 member stars were identified with Gaia DR2 (Zuckerman et al. 2019). After the release of Gaia-EDR3 (Gaia Collaboration et al. 2021), its membership was extended to 164 stars, and its distance was determined to be ~ 108 pc (Galli et al. 2021). This region was later expanded to define the Fornax-Horologium (FH) association of 329 candidate members with XFOR as the core cluster and a halo of stars surrounding the cluster (Kerr et al. 2022). The FH is located in the Austral Complex, which is one of the nearest young stellar populations and contains other associations, including Tuc-Hor, Carina, and Columba (Kerr et al. 2022).

Open clusters are gravitationally bound, while young moving groups are not (e.g., Gagné 2024). Initially, XFOR was identified as one of the few young open clusters in the solar neighbour-

¹ Date are from <https://exoplanet.eu/catalog/>.

hood. Hunt & Reffert (2024) reported that only 11% of the open clusters within 250 pc can be identified as bound open clusters by their Jacobi radius, and they classified XFOR as a moving group instead of an open cluster. Kerr et al. (2022) reported that XFOR is likely in the virialised state and that the FH consists of a probably dissolving cluster with a large low-density halo. Therefore, while the FH is currently not an overdense configuration, it likely formed in a much more compact configuration when we trace the motion of the stars back in time. By contrast, there are young star associations (1–5 Myr) in which stars formed in relatively loose environments. While XFOR is no longer an open cluster, it therefore previously was in a gravitationally bound state and is now dissolving into a moving group.

The age of the FH as determined from isochrones, dynamics, and X-ray emissions, agrees well within 30–40 Myr (Galli et al. 2021; Kerr et al. 2022; Mamajek 2016). Known young associations and moving groups within 150 pc either have ages younger than 30 Myr, such as TW Hydrae (~ 10 Myr, Bell et al. 2015), β Pictoris (~ 22 Myr, Shkolnik et al. 2017), Columba, and Carina (~ 26 Myr, Kerr et al. 2022), or older than 40 Myr, such as Tuc-Hor (~ 46 Myr, Kerr et al. 2022), AB Doradus (~ 150 Myr, Bell et al. 2015), and Argus (40–50 Myr, Zuckerman 2019). Therefore, the FH provides a valuable opportunity for studying planetary systems at ages between 30 and 40 Myr. The rich abundance of M dwarfs with warm debris discs in XFOR indicates that this cluster has gone through an active companion formation (Zuckerman et al. 2019). Its young age and proximity make it well suited for direct-imaging surveys of exoplanets.

During the expansion and dissolution of the FH, there were likely frequent stellar encounters and flybys. These dynamical interactions have a significant impact on the formation and survivability of wide-orbit low-mass stellar and substellar companions. On the one hand, frequent stellar encounters in a dense environment may trigger more gravitational instability (Krumholz et al. 2012) and promote the formation of wide-orbit companions. On the other hand, they can also cause orbit instability and eject companions from their natal systems (Parker & Quanz 2012; van Elteren et al. 2019).

The FH occupies a unique parameter space in terms of age and cluster evolution. We are therefore conducting a direct imaging survey of stars in the FH (PI: P. Liu). We selected stars with G brighter than 12 mag and a renormalised unit weight error (RUWE) smaller than 1.4 to filter out possible unresolved binaries. We checked the Tycho-2 (Høg et al. 2000), Gaia DR3 (Gaia Collaboration et al. 2021) and Hipparcos-Gaia (Brandt 2021) catalogues and excluded accelerating stars with possible stellar companions at small separations predicted by the COPAINS tool (Fontanive et al. 2019). The sample contains 18 stars from the central core XFOR compiled in Galli et al. (2021) and 31 stars from the halo compiled in Kerr et al. (2022). The mass of the sample ranges between 0.8 and $2.4 M_{\odot}$ (Kerr et al. 2022). The observations were taken with the Spectro-Polarimetric High-contrast Exoplanet REsearch (SPHERE) instrument (Beuzit et al. 2019) in pupil-tracking mode. We used the angular differential imaging (ADI) strategy (Marois et al. 2006). We present the first companion imaged in this survey: an object at the hydrogen-burning limit orbiting HD 24121.

2. Observations and data analysis

The observations of HD 24121 were conducted in the dual-band imaging mode with SPHERE/IRDIS in the $H2$ and $H3$ filters. We used the N_ALC_YJH_S coronagraph to mask the central star. The first-epoch observations of HD 24121 were taken on

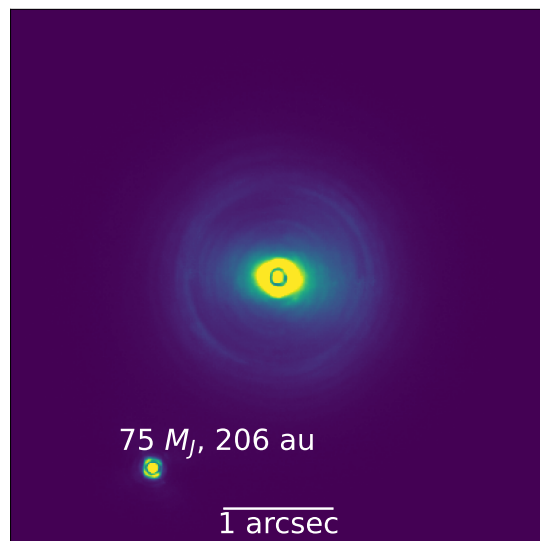


Fig. 1: Coronagraphic image of HD 21411 at the first epoch of SPHERE observations. The brown dwarf companion is the point source in the south-east direction. North is up, and east is to the left.

4 Oct 2023 with a total time of 1.5 h. The science time was 1.1 h with a detector integration time (DIT) = 32 s and a number of DIT (NDIT) = 1 for each exposure. The airmass ranged from 1.04 to 1.08. The total field-of-view rotation was $42^{\circ}18'$. The seeing varied between $0''.46$ and $0''.70$. The second-epoch observations of HD 24121 were taken on 10 Nov 2024 with a total duration of 35 min. The observation mode was set to the same mode as for the first epoch. The science time was 0.16 h with DIT = 32 s and NDIT = 1. The airmass ranged from 1.063 to 1.056. The total field-of-view rotation was $5^{\circ}57'$. The seeing varied between $0''.63$ and $0''.96$. In each epoch, we also took two separate non-coronagraphic exposures of the central star of DIT = 6 s and NDIT = 1 with the neutral density filter ND_1.0 at the beginning and end of observations.

We reduced the raw images using the ESO pipeline for SPHERE wrapped in a Python script (Vigan 2020). The companion is bright enough to be seen in each preprocessed frame. It is at a distance of ~ 2 arcsec in the south-east direction of the central star, as shown in the de-rotated and stacked image of the first epoch in Fig. 1. We also applied classical ADI to the data cube and did not detect any other sources.

3. Results

This companion was also detected by Gaia with the Gaia ID of Gaia DR3 4855032616243433984 (Gaia Collaboration et al. 2021). The Gaia ID of the primary star is Gaia DR3 4855032616243433856. They are high proper motion sources that move in similar directions in the Gaia catalogue. Their parallax agrees within 1σ , while the difference in proper motion is larger than 2σ : -0.6 ± 0.3 mas yr $^{-1}$ in RA and -2.6 ± 0.5 mas yr $^{-1}$ in Dec, which is likely due to the orbital motion of the companion. The primary star has a spectral type of G3 (Zuckerman et al. 2019) with a mass of $\sim 1.06 M_{\odot}$ (Kerr et al. 2022). Table 1 summarises the properties of this system, updated with our SPHERE observations.

Table 1: Properties of the HD 24121 AB system

| Property | Primary | Secondary |
|--|-------------------------------|--|
| Age (Myr) ^a | 30 – 40 | ... |
| Parallax (mas) ^b | 10.17 ± 0.01 | 9.67 ± 0.53 |
| $\mu_{\alpha} \cos(\delta)$ (mas yr ⁻¹) ^b | 38.72 ± 0.01 | 38.13 ± 0.34 |
| μ_{δ} (mas yr ⁻¹) ^b | -2.64 ± 0.01 | -5.22 ± 0.48 |
| Sep ^c (mas, 2016.0) | - | 2071.2 ± 0.4 |
| PA ^c (deg, 2016.0) | - | 146.31 ± 0.01 |
| Sep ^d (mas, 2023-10-04) | - | 2082 ± 4 |
| PA ^d (deg, 2023-10-04) | - | 146.56 ± 0.15 |
| Sep ^d (mas, 2024-11-10) | - | 2082 ± 4 |
| PA ^d (deg, 2024-11-10) | - | 146.62 ± 0.15 |
| Gaia G (mag) | 9.628 ± 0.003 | 17.28 ± 0.01 |
| SPHERE $\Delta H2$ (mag) ^e | - | 5.07 ± 0.05 |
| SPHERE $\Delta H3$ (mag) ^e | - | 4.98 ± 0.05 |
| 2MASS J (mag) | 8.656 ± 0.024 | - |
| 2MASS H (mag) | 8.383 ± 0.046 | - |
| 2MASS K (mag) | 8.312 ± 0.024 | - |
| T_{eff} (K) ^e | 5819 ± 13 | 2972 ⁺²²⁰ ₋₁₉₈ |
| $\log(L/L_{\odot})$ (dex) ^e | 0.012 ± 0.001 | -2.48 ± 0.06 |
| Mass | 1.06 M_{\odot} ^f | 74.9 ± 7.5 M_{J} ^e |

Notes. ^(a) There is no conclusive age for XFOR, but the latest age estimate is about 30 Myr (Galli et al. 2021; Kerr et al. 2022). We adopted a conservative age range of 30 – 40 Myr. ^(b) Both of them have Gaia astrometry data, and we present them here. ^(c) Separation and position angle in the Gaia reference epoch 2016.0. ^(d) Separation and position angle measured in SPHERE observations. ^(e) This work. ^(f) Kerr et al. (2022).

3.1. Astrometry

We fitted a 2D Gaussian to each individual SPHERE frame and took the mean value as the measured position and the standard deviation as the fitting uncertainty. We also included the uncertainty from the pixel scale, centring, distortion, true north angle, and pupil offset following the astrometry calibration provided in the latest SPHERE User manual² and by Maire et al. (2021). The results are presented in Table 1. We present the relative astrometry measured with SPHERE in 2023 and 2024 in Fig. 2. We also include the relative positions of HD 24121B to HD 24121 in the Gaia reference epoch 2016.0. It is comoving with the central star between 2023 and 2024. The position difference between the Gaia and SPHERE epochs is likely due to the orbital motion of HD 24121B over 8 years. The projected separation is about 200 au given the measured angular separation of $\sim 2''$ at a distance of 98 pc.

3.2. Photometry

We performed aperture photometry of HD 24121B in the de-rotated and stacked image and subtracted the local sky background. We calculated the signal-to-noise ratio (S/N) of HD 24121B by performing photometry on all apertures of the same size at the same separation as the source, but at different position angles, except for the aperture on the companion. Then, we took the three σ clipped standard deviation as the noise and the average as the local sky background. We also performed aperture photometry on the non-coronagraphic image with the same aperture radius to measure the star flux. Then, we con-

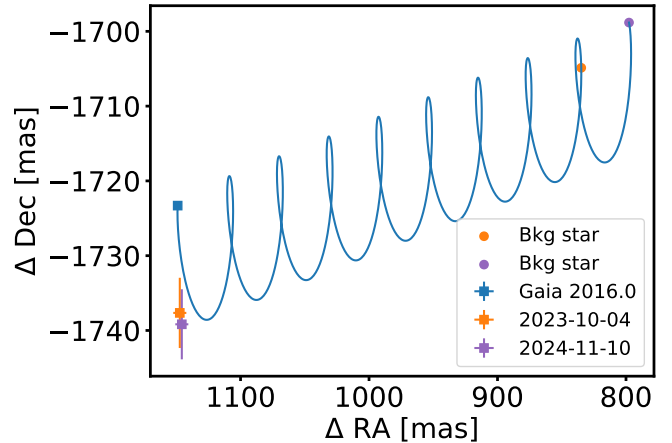


Fig. 2: Relative positions of HD 24121B to the central star. The blue trajectory shows the relative position of a static background star over time, starting from the Gaia reference epoch 2016.0. The orange and purple dots on the track indicate the expected positions at epochs 2023-10-04 and 2024-11-10 if HD 24121B was a static background star.

verted the flux contrast into magnitude contrast. The magnitude contrasts measured in the first epoch are $\Delta H2 = 5.09 \pm 0.11$ mag and $\Delta H3 = 4.99 \pm 0.11$ mag. The magnitude contrasts measured in the second epoch are $\Delta H2 = 5.07 \pm 0.05$ mag and $\Delta H3 = 4.98 \pm 0.05$ mag. They agree with each other within 1σ without discernible variability.

To estimate the effective temperature of HD 24121B, we fitted the spectral energy distribution (SED) using SPECIES (Stolker et al. 2020). Data are available in three photometric bands: Gaia G, and SPHERE H2 and H3. We measured the contrasts of the companion to the central star in H2 and H3. To convert the SPHERE band contrasts into the apparent magnitudes of the companion, we first performed synthetic photometry on the central star. We fitted the SED of the host star using its GALEX, Tycho, SDSS, Gaia, 2MASS, and WISE photometric data with the BT-Settl-CIFIST models (Allard et al. 2013). We fitted $T_{\text{eff}} = 5819$ K, similar to 5805 K reported in Gaia. The SED fitting results of the primary star can be found in Appendix A. Then, we measured the primary magnitude in H2 and H3 by applying synthetic photometry on the best-fit model spectrum. Adding the contrasts measured from direct imaging, we obtained the apparent magnitude of HD 24121B in H2 and H3.

Then, we used two evolutionary models for warm brown dwarfs to fit its SED: BT-Settl (Allard et al. 2003) and AMES-DUSTY (Allard et al. 2001; Chabrier et al. 2000). We included error inflation factors in the fitting because the uncertainty from the synthetic photometry is underestimated. We derived similar results for the two models. BT-Settl has slightly smaller residuals in the SED fitting, and therefore, we present its best-fit spectra in Fig. 3 and the posterior distribution in Appendix A. We fitted $T_{\text{eff}} = 2972^{+220}_{-198}$ K and $\log(L/L_{\odot}) = -2.48 \pm 0.06$ dex for the companion.

3.3. Orbital fitting

To find plausible orbits for this system, we used ORBITIZE (Blunt et al. 2020) to fit the relative astrometry of HD 24121B and HD 24211 by combining the Gaia reference epoch of 2016.0

² <https://www.eso.org/sci/facilities/paranal/instruments/sphere/doc.html>

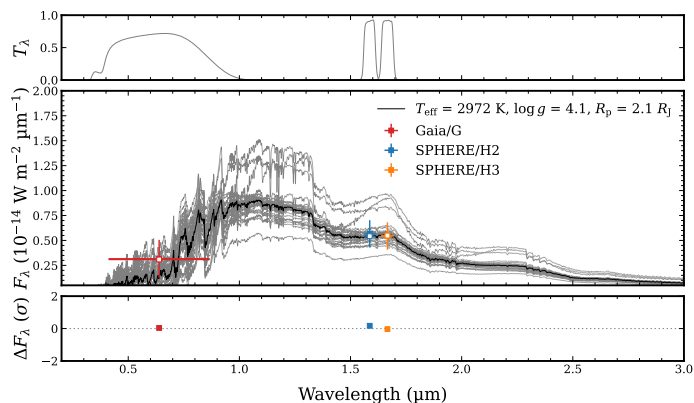


Fig. 3: SED fitting of the companion, combining the Gaia G , and SPHERE $H2$ and $H3$ photometric bands using BT-Settl atmospheric models. The filled squares are the measured photometric data with error bars, and the open squares are the modelled photometric data. The grey lines are 30 spectra randomly drawn from the posterior distributions. The upper panel shows the transmission of photometric bands, and the lower panel shows the residuals in σ .

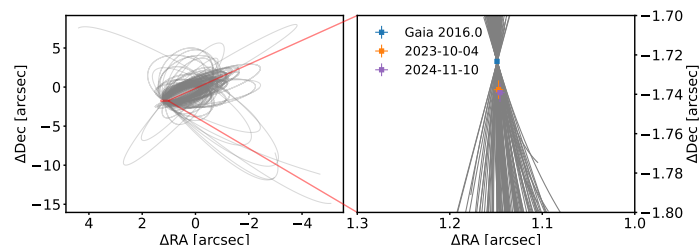


Fig. 4: Fitted orbits of HD 24121B. We show 100 random orbits drawn from the posterior of the fit.

and the two SPHERE epochs. We adopted a parallax of 10.17 ± 0.01 mas for the primary star from Gaia DR3, and we assumed a total mass of $1.13 \pm 0.1 M_{\odot}$. The fitted orbits are shown in Fig. 4. The posterior distributions of orbital parameters are presented in Appendix B. We find a semi-major axis of ~ 205 au and a well-constrained inclination of $70^{\circ}4^{+9.6}_{-19.1}$. The orbital period is ~ 2745 year. We find a high eccentricity for HD 24121B, with a median of 0.6 and a peak of 0.9, according to its posterior distribution.

We calculated the fitted orbital velocity of HD 24121B in the Gaia reference epoch and derived the velocity in RA (v_{ra}) = -0.3 ± 0.4 mas yr $^{-1}$ and the velocity in Dec (v_{dec}) = -1.8 ± 0.4 mas yr $^{-1}$. The posterior distribution is presented in Appendix B. The fitted orbital velocity matches the Gaia measured proper motion difference within $1-2\sigma$. Therefore, the two sources are very likely in a gravitationally bound system.

3.4. Companion mass estimation

The dynamical mass of the companion cannot be constrained in the orbital fitting due to the small orbit coverage. There is no evidence of Gaia acceleration in either source: Their RUWE is smaller than 1. There is no proper motion anomaly between the Gaia and Hipparcos catalogue (Brandt 2021). Therefore, we estimated the mass from photometry using the rejection-sampling method (e.g., Dupuy & Liu 2017). With a bolometric luminosity of -2.48 ± 0.06 dex from the SED fitting and an age of 32.4 ± 1.3 Myr (Kerr et al. 2022), the derived mass is $72.2 \pm$

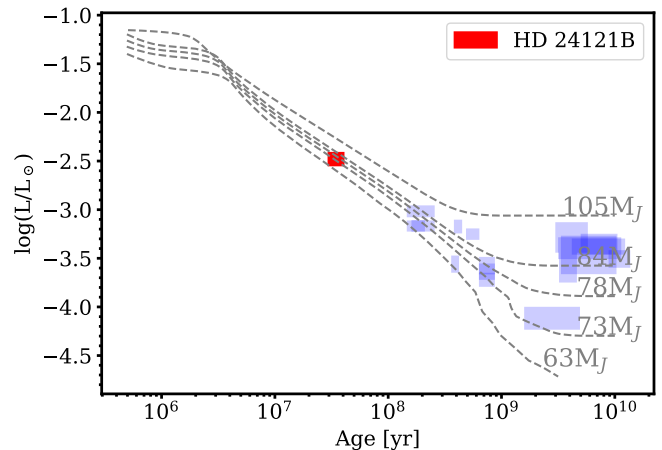


Fig. 5: Evolutionary tracks of low-mass stars and brown dwarfs from the BCAH15 models. Hydrogen-burning stars reach stable luminosities after a certain contraction time, while brown dwarfs continue to cool. The red square indicates the luminosity (1σ) and age (30 – 40 Myr) range of HD 24121B. The blue squares show the companions at the hydrogen-burning limit from the Gaia ultracool dwarf companion catalogue, which includes objects within 100 pc (Baig et al. 2024). HD 24121B is located at the hydrogen-burning limit between low-mass stars and brown dwarfs, and it is much younger than the other companions.

$6.4 M_J$ using the BT-Settl evolutionary models. With a broader uniform age distribution between 30 and 40 Myr, the derived mass is $74.9 \pm 7.5 M_J$. We obtained consistent results with the BCAH15 model (Baraffe et al. 2015). As demonstrated in Fig. 5, HD 24121 straddles the region between brown dwarfs and low-mass hydrogen-burning stars in the evolutionary tracks.

4. Discussions and conclusions

We presented a companion of HD 24121, the object HD 24121B. With a mass of $74.9 \pm 7.5 M_J$, HD 24121B can serve as a benchmark object in characterising the evolutionary models of low-mass stars and brown dwarfs at the hydrogen-burning boundary. There are not many directly imaged low-mass stellar and substellar companions at the age of 30 Myr. Almost all of the benchmark brown dwarf companions at the hydrogen-burning limit were found in relatively old systems such as HD 72946B ($72.4 \pm 1.6 M_J$, 0.9 – 3 Gyr, Maire et al. 2020), HR 7672B ($\sim 68.7 M_J$, 2.5 Gyr, Crepp et al. 2012), and HD 4747B ($70 \pm 1.6 M_J$, 2.3 ± 1.4 Gyr Peretti et al. 2019), and those compiled in the Gaia ultracool dwarf companion sample (Baig et al. 2024). Most of the directly imaged companions in the literature that are younger than 30 Myr have masses lower than $70 M_J$, which is likely due to a selection bias. Nevertheless, HD 24121B provides a unique age range for studying evolutionary models at the hydrogen-burning limit. At the age of 30 Myr with a mass of $75 M_J$, HD 24121B is about to start lithium burning according to the BT-Settl and BCAH15 models. A future spectroscopic characterisation of HD 24121B can measure its lithium abundance.

The formation of HD 24121B is also an intriguing question. It is challenging to form such a heavy companion at 200 au by core accretion or even pebble accretion (Chambers 2021; Savvidou & Bitsch 2023). Disc fragmentation triggered by gravitational instability and binary-like cloud fragmenta-

tion are probably the most favourable formation mechanisms here. They can produce brown dwarfs and low-mass hydrogen-burning stellar companions around Sun-like stars (Stamatellos & Whitworth 2009). Moreover, subsequent dynamical effects such as fragment-fragment scattering are efficient powers to modify the orbital parameters of companions (Hall et al. 2017; Forgan et al. 2018). The fragment-fragment scattering can populate the companions to a broader semi-major axis range such as over $10^2 - 10^3$ au (Forgan et al. 2018). Dynamical evolution including fragment-fragment scattering and multi-object scattering also result in a relatively higher eccentricity for wide-orbit companions or even planet ejection and recapturing (Forgan et al. 2015), which agrees with the high eccentricity we derived for HD 24121B. Hwang et al. (2022) reported that wide stellar binaries have a uniform eccentricity distribution for separations within 200 au. A similar trend has been found for brown dwarfs within 100 au: They have a broad peak at an eccentricity of 0.6–0.9 (Bowler et al. 2020). Therefore, HD 24121B is likely formed by disc or cloud fragmentation, followed by a dynamical evolution, before it reached its current orbit.

The possible dynamical scattering might result from interactions with another companion in the same system. To estimate the upper mass limit of the potential another companion, we calculated the 5σ contrast curve of the dataset of the epoch 4 Oct 2023 and reached a sensitivity of $3 M_J$ beyond $\sim 1''.5$. Therefore, this companion is probably smaller than $3 M_J$ or at a smaller separation with a higher mass if it has survived in the same system. Because HD 24121 is located in the core cluster of the FH, dynamical scattering between HD 24121 and other stars may also have been possible. The core cluster of the FH is a dissolving open cluster, and its core region is about one order of magnitude denser than the local disc stellar density (Zuckerman et al. 2019). When we trace the motion of stars back, the chances of stellar encounters and flybys are probably much higher than in the current stage.

A composition and abundance comparison of HD 24121 and HD 24121B can give more clues about the formation of HD 24121B, such as the C/O ratio, which can serve as an indicator of its formation location in the disc and evidence of gas accretion (e.g., Öberg et al. 2011). Recently, the carbon isotopologue ratio was proposed as a probe to distinguish low-mass planet and brown dwarf formation pathways (Zhang et al. 2021a,b; de Regt et al. 2024; González Picos et al. 2025). Although the central star HD 24121 may be too hot for us to measure its carbon isotopologue ratio, high-resolution spectroscopic observations of HD 24121B in the near-infrared band can constrain its isotopologue ratio, which can then be compared with that of other brown dwarfs. Spectroscopic observations can also provide the spin-rate measurement of HD 24121B from broadened spectral lines, which will provide indications about its angular momentum evolution (Bouvier et al. 2014; Schwarz et al. 2016). We therefore recommend follow-up spectroscopic observations to characterise HD 24121B. It can serve as a benchmark object for studying the evolutionary models and formation mechanisms of low-mass stellar and substellar companions.

Acknowledgements. We are grateful to W. K. M. Rice for insightful discussions that contributed to the development of this work. RK acknowledges the support from the Dunlap Institute, which is funded through an endowment established by the David Dunlap family and the University of Toronto. Based on observations collected at the European Organisation for Astronomical Research in the Southern Hemisphere under ESO programmes 112.25SC.001 and 114.2776.001. This research made use of *ASTROPY*, a community-developed core PYTHON package for Astronomy (Astropy Collaboration et al. 2013, 2018), *NUMPY* (Harris et al. 2020) and *MATPLOTLIB*, a Python library for publication quality graphics (Hunter 2007).

References

- Allard, F., Guillot, T., Ludwig, H.-G., et al. 2003, in IAU Symposium, Vol. 211, Brown Dwarfs, ed. E. Martín, 325
- Allard, F., Hauschildt, P. H., Alexander, D. R., Tamanai, A., & Schweitzer, A. 2001, *ApJ*, 556, 357
- Allard, F., Homeier, D., Freytag, B., Schaffnerberger, W., & Rajpurohit, A. S. 2013, *Memorie della Societa Astronomica Italiana Supplementi*, 24, 128
- Astropy Collaboration, Price-Whelan, A. M., Sipőcz, B. M., et al. 2018, *AJ*, 156, 123
- Astropy Collaboration, Robitaille, T. P., Tollerud, E. J., et al. 2013, *A&A*, 558, A33
- Baig, S., Smart, R. L., Jones, H. R. A., et al. 2024, *MNRAS*, 533, 3784
- Baraffe, I., Homeier, D., Allard, F., & Chabrier, G. 2015, *A&A*, 577, A42
- Bell, C. P. M., Mamajek, E. E., & Naylor, T. 2015, *MNRAS*, 454, 593
- Beuzit, J. L., Vigan, A., Mouillet, D., et al. 2019, *A&A*, 631, A155
- Biller, B. A., Liu, M. C., Wahhaj, Z., et al. 2010, *ApJ*, 720, L82
- Biller, B. A., Liu, M. C., Wahhaj, Z., et al. 2013, *ApJ*, 777, 160
- Blunt, S., Wang, J. J., Angelo, I., et al. 2020, *AJ*, 159, 89
- Boss, A. P. 1997, *Science*, 276, 1836
- Bouvier, J., Matt, S. P., Mohanty, S., et al. 2014, in *Protostars and Planets VI*, ed. H. Beuther, R. S. Klessen, C. P. Dullemond, & T. Henning, 433
- Bowler, B. P., Blunt, S. C., & Nielsen, E. L. 2020, *AJ*, 159, 63
- Brandt, T. D. 2021, *ApJS*, 254, 42
- Chabrier, G., Baraffe, I., Allard, F., & Hauschildt, P. 2000, *ApJ*, 542, 464
- Chambers, J. 2021, *ApJ*, 914, 102
- Crepp, J. R., Gonzales, E. J., Bechter, E. B., et al. 2016, *ApJ*, 831, 136
- Crepp, J. R., Johnson, J. A., Fischer, D. A., et al. 2012, *ApJ*, 751, 97
- de Regt, S., Gandhi, S., Snellen, I. A. G., et al. 2024, *A&A*, 688, A116
- Desidera, S., Chauvin, G., Bonavita, M., et al. 2021, *A&A*, 651, A70
- Dias, W. S., Alessi, B. S., Moitinho, A., & Lépine, J. R. D. 2002, *A&A*, 389, 871
- Dupuy, T. J. & Liu, M. C. 2017, *ApJS*, 231, 15
- Fontanive, C., Mužić, K., Bonavita, M., & Biller, B. 2019, *MNRAS*, 490, 1120
- Forgan, D., Parker, R. J., & Rice, K. 2015, *MNRAS*, 447, 836
- Forgan, D. H., Hall, C., Meru, F., & Rice, W. K. M. 2018, *MNRAS*, 474, 5036
- Fujii, M. S. & Hori, Y. 2019, *A&A*, 624, A110
- Gagné, J. 2024, *PASP*, 136, 063001
- Gaia Collaboration, Brown, A. G. A., Vallenari, A., et al. 2021, *A&A*, 649, A1
- Galli, P. A. B., Bouy, H., Olivares, J., et al. 2021, *A&A*, 654, A122
- González Picos, D., Snellen, I. A. G., de Regt, S., et al. 2025, *A&A*, 693, A298
- Gratton, R., Bonavita, M., Mesa, D., et al. 2024, *A&A*, 685, A119
- Gratton, R., Bonavita, M., Mesa, D., et al. 2025, *A&A*, 694, A175
- Hall, C., Forgan, D., & Rice, K. 2017, *MNRAS*, 470, 2517
- Harris, C. R., Millman, K. J., van der Walt, S. J., et al. 2020, *Nature*, 585, 357
- Høg, E., Fabricius, C., Makarov, V. V., et al. 2000, *A&A*, 355, L27
- Hunt, E. L. & Reffert, S. 2024, *A&A*, 686, A42
- Hunter, J. D. 2007, *Computing In Science & Engineering*, 9, 90
- Hwang, H.-C., Ting, Y.-S., & Zakamska, N. L. 2022, *MNRAS*, 512, 3383
- Kerr, R., Kraus, A. L., Murphy, S. J., et al. 2022, *ApJ*, 941, 143
- Konopacky, Q. M., Marois, C., Macintosh, B. A., et al. 2016, *AJ*, 152, 28
- Krumholz, M. R., Klein, R. I., & McKee, C. F. 2012, *ApJ*, 754, 71
- Maire, A. L., Baudino, J. L., Desidera, S., et al. 2020, *A&A*, 633, L2
- Maire, A.-L., Langlois, M., Delorme, P., et al. 2021, *Journal of Astronomical Telescopes, Instruments, and Systems*, 7, 035004
- Mamajek, E. E. 2016, in IAU Symposium, Vol. 314, *Young Stars & Planets Near the Sun*, ed. J. H. Kastner, B. Stelzer, & S. A. Metchev, 21–26
- Marois, C., Lafrenière, D., Doyon, R., Macintosh, B., & Nadeau, D. 2006, *ApJ*, 641, 556
- Nielsen, E. L., De Rosa, R. J., Macintosh, B., et al. 2019, *AJ*, 158, 13
- Nielsen, E. L., Liu, M. C., Wahhaj, Z., et al. 2012, *ApJ*, 750, 53
- Öberg, K. I., Murray-Clay, R., & Bergin, E. A. 2011, *ApJ*, 743, L16
- Parker, R. J. & Quanz, S. P. 2012, *MNRAS*, 419, 2448
- Peretti, S., Ségransan, D., Lavie, B., et al. 2019, *A&A*, 631, A107
- Pollack, J. B., Hubickyj, O., Bodenheimer, P., et al. 1996, *Icarus*, 124, 62
- Savvidou, S. & Bitsch, B. 2023, *A&A*, 679, A42
- Schwarz, H., Ginski, C., de Kok, R. J., et al. 2016, *A&A*, 593, A74
- Shkolnik, E. L., Allers, K. N., Kraus, A. L., Liu, M. C., & Flagg, L. 2017, *AJ*, 154, 69
- Stamatellos, D. & Whitworth, A. P. 2009, *MNRAS*, 392, 413
- Stolker, T., Quanz, S. P., Todorov, K. O., et al. 2020, *A&A*, 635, A182
- van Elteren, A., Portegies Zwart, S., Pelupessy, I., Cai, M. X., & McMillan, S. L. W. 2019, *A&A*, 624, A120
- Vigan, A. 2020, *vlt-sphere: Automatic VLT/SPHERE data reduction and analysis*
- Wahhaj, Z., Liu, M. C., Biller, B. A., et al. 2011, *ApJ*, 729, 139
- Zhang, Y., Snellen, I. A. G., Bohn, A. J., et al. 2021a, *Nature*, 595, 370
- Zhang, Y., Snellen, I. A. G., & Mollière, P. 2021b, *A&A*, 656, A76
- Zheng, X., Kouwenhoven, M. B. N., & Wang, L. 2015, *MNRAS*, 453, 2759
- Zuckerman, B. 2019, *ApJ*, 870, 27
- Zuckerman, B., Klein, B., & Kastner, J. 2019, *ApJ*, 887, 87

Appendix A: SED fitting

We present the posterior distribution of the SED fitting of the primary star in Fig. A.1. We included error inflation into fitting because the uncertainty in GALEX and SDSS photometric data is likely underestimated. No infrared excess is detected.

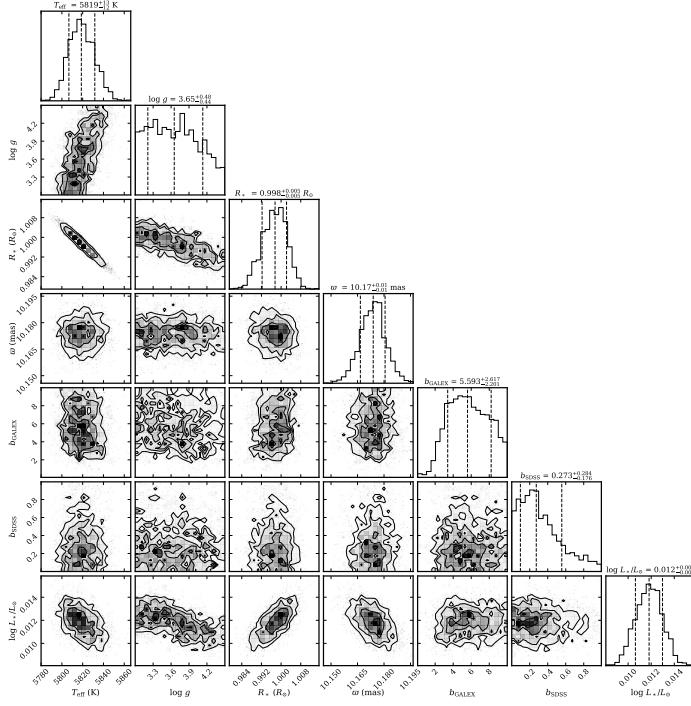
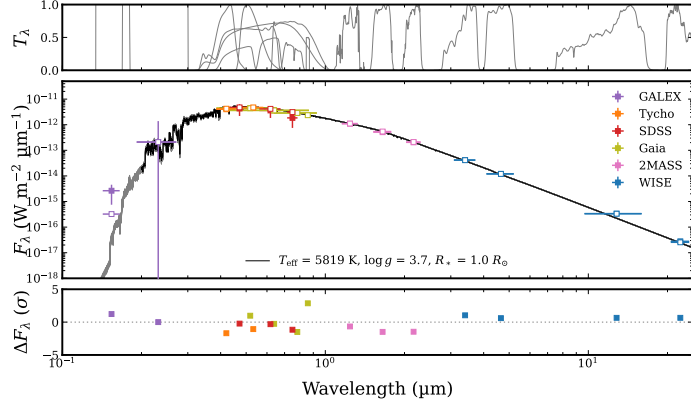


Fig. A.1: SED fitting of the central star using BT-Settl-CIFIST models. Upper panel: the filled squares with errorbar are the measured photometric data and the open squares are the modelled photometric data. The black line is the optimised model spectrum and the grey lines are 30 spectra randomly drawn from the posterior distributions. Lower panel: posteriors distributions of SED fitting. b_{GALEX} and b_{SDSS} are the inflation factors of the GALEX and SDSS photometric data.

The posterior distribution of the SED fitting of the companion is shown in Fig. A.2.

Appendix B: Orbital fitting

We show the posterior distribution of orbital parameters of H 24121B in Fig. B.1.

We show the posterior distribution of orbital velocity from ORBITIZE fitting in the Gaia reference epoch 2016.0 in Fig. B.2.

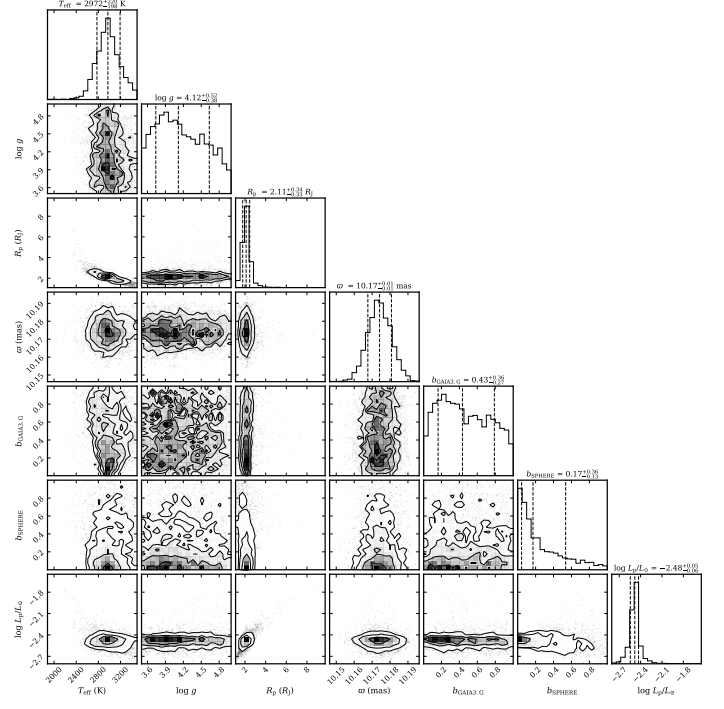


Fig. A.2: Posterior distribution of the SED fitting of the companion using BT-Settl models. $b_{GALEX,G}$ and b_{SPHERE} are the inflation factors of the Gaia and SPHERE photometric data

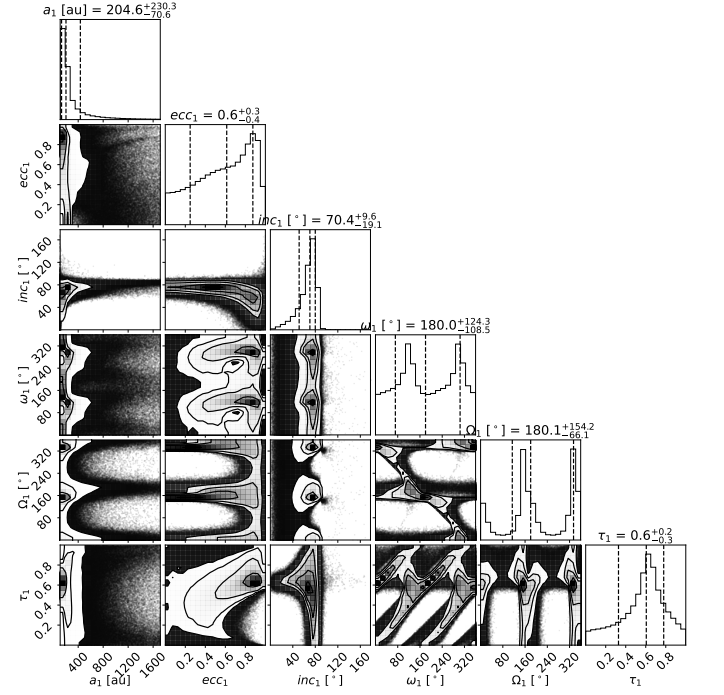


Fig. B.1

The orbital velocity agrees with the proper motion difference measured by Gaia within $1-2\sigma$.

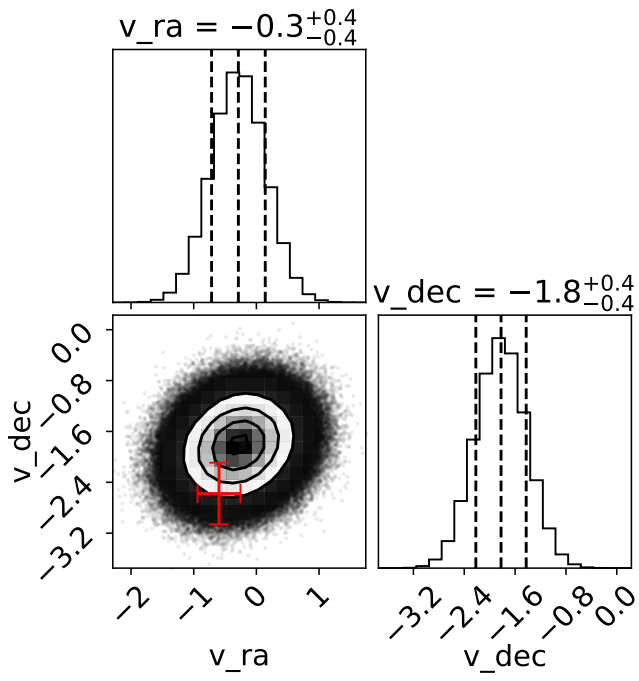


Fig. B.2: Posterior distribution of the orbital velocity of HD 24121B in the Gaia reference epoch. The units are in mas yr^{-1} . The red data point is the proper motion difference from Gaia.